



# **NUMERICAL EVALUATION OF NONLINEAR OPTICAL PROPERTIES OF SPIRAL-SHAPED CERAMIC OPTICAL FIBERS**

Lappeenranta-Lahti University of Technology LUT

Master's Program in Computational Engineering, Master's Thesis

2024

Bipul Biswas

Examiners: Professor Lasse Lensu

Associate Professor Erik Vartiainen

# ABSTRACT

Lappeenranta-Lahti University of Technology LUT  
School of Engineering Science  
Computational Engineering

Bipul Biswas

## **Numerical evaluation of nonlinear optical properties of spiral-shaped ceramic optical fibers**

Master's thesis

2024

43 pages, 19 figures, 3 tables, no appendices

Examiners: Professor Lasse Lensu and Associate Professor Erik Vartiainen

Keywords: Photonic Crystal Fiber, Ceramics Materials, Spiral-shaped, Beat Length, Optical Nonlinearity, Birefringence

A spiral-shaped photonic crystal fiber (SS-PCF) is described in this master's thesis. The focus of this thesis is to use a fine mesh and the finite element method (FEM) to predict the elemental properties of optical transmission, such as optical nonlinearity, confinement loss, beat length, numerical aperture, birefringence, and effective mode area. Separately employed as core materials, gallium phosphide (GaP), graphene, and tellurite exhibit greater performance than earlier works. Graphene provides extremely high optical nonlinearity which is six orders of magnitude higher than GaP and seven orders of magnitude higher than tellurite at the wavelength range of 0.1 to 1.5  $\mu\text{m}$ . To the best of my knowledge, this SS-PCF is the first to test the performance of these three ceramic objects in optical nonlinear applications. In actuality, the structure's evanescent fields aid in the modeling process and display a performance outline with a high birefringence of 0.33, a high numerical aperture of 0.86, and a very low confinement loss of  $2.86 \times 10^{-9}$  dB/m. All these results are relevant in nonlinear applications including biological imaging, sensing, supercontinuum optics, polarization maintenance, optical parameter amplification, and others.

## ACKNOWLEDGEMENTS

I am thankful for the opportunities that have allowed me to reach this point in my studies. I am grateful for the abundance in my life and the many positive aspects that have contributed to my journey so far. I would like to express my utmost admiration and sincere respect to my supervisor Associate Prof. Erik Vartiainen, and my co-supervisor Prof. Lasse Lensu, Department of Data-Centric Engineering, Lappeenranta-Lahti University of Technology (LUT), for their kindness as well as for their helpful advice, and continuous support of my research activities. Without their patience, encouragement, and careful review support, this thesis would not have been possible. I am pleased to extend my heartiest respect and indebtedness to our honorable teachers Prof. Heikki Kalviainen, Prof. Lassi Roininen, and Prof. Satu-Pia Reinikainen of the same Department for their valuable suggestions and inspiration throughout my studies. I convey my appreciation to all the members of our Data-Centric Engineering Department. Last but not least, I would like to express my sincere admiration for my beloved parents, sister, and brother for their moral support and invaluable encouragement in helping me reach this stage.

Declaration of AI use: During the preparation of this master's thesis, Bipul Biswas, the author of the thesis, used Grammarly in order to find typographical and grammatical errors. After using Grammarly, the author reviewed and edited the content and takes full responsibility for the thesis content.

Lappeenranta, June 10, 2024

*Bipul Biswas*

## LIST OF ABBREVIATIONS

2-D	two-dimensional
Br	birefringence
CL	confinement loss
EA	effective area
EMI	effective mode index
FDTD	finite difference time domain
FEM	finite element method
FV-FEM	full vector finite element method
FWM	four-wave mixing
GaP	gallium phosphide
HOF	holey optical fiber
IG	index guiding
NA	numerical aperture
NOF	nonlinear optical fibers
OCT	optical coherence tomography
PBG	photonic band gap
PCF	photonic crystal fiber
PDEs	partial differential equations
PML1	perfectly matched layer-1
PWE	partial wave expansion
RI	refractive index
SPM	self-phase modulation
SPR	surface Plasmon resonance
SS-PCF	spiral-shaped photonic crystal fiber
TIR	total internal reflection

## LIST OF SYMBOLS

$A_{\text{eff}}$	effective area
$d$	air hole diameter
$\gamma$	nonlinearity
$\eta$	power fraction
$L_b$	beat length
$L_c$	confinement loss
$\lambda$	operating wavelength

# CONTENTS

<b>1</b>	<b>INTRODUCTION</b>	<b>8</b>
1.1	Background . . . . .	8
1.2	Objectives and delimitations . . . . .	10
1.3	Structure of the thesis . . . . .	11
<b>2</b>	<b>PRINCIPLES OF PHOTONIC CRYSTAL FIBERS</b>	<b>12</b>
2.1	Literature Review . . . . .	12
2.2	Light Capturing Operation of Photonic Crystal Fiber . . . . .	14
2.2.1	Total Internal Reflection . . . . .	14
2.2.2	Photonic Bandgap Guiding . . . . .	15
2.3	Nonlinear Photonic Crystal Fiber in Supercontinuum Generation . . . . .	15
2.4	Nonlinear Optical Fiber in Four-Wave Mixing . . . . .	16
2.5	Nonlinear Optical Fiber in Self-phase Modulation . . . . .	17
2.6	Advantages of Photonic Crystal Fiber in Nonlinear Applications . . . . .	18
2.7	Nonlinear Optical Fiber in a Nutshell . . . . .	18
<b>3</b>	<b>DESIGN OF SPIRAL-SHAPED PHOTONIC CRYSTAL FIBER</b>	<b>20</b>
3.1	Geometry . . . . .	20
3.2	Simulation Criteria . . . . .	21
3.3	Finite Element Method . . . . .	21
3.4	Fabrication Process . . . . .	22
<b>4</b>	<b>NUMERICAL CHARACTERIZATION</b>	<b>24</b>
4.1	Refractive Index . . . . .	24
4.2	Birefringence . . . . .	24
4.3	Beat Length . . . . .	25
4.4	Power Fraction . . . . .	25
4.5	Confinement Loss . . . . .	25
4.6	Effective Mode Area . . . . .	26
4.7	Numerical Aperture . . . . .	26
4.8	Nonlinearity . . . . .	26
<b>5</b>	<b>RESULTS</b>	<b>28</b>
5.1	Simulation Results of the Proposed Optical Fiber Structure . . . . .	28
5.2	Summary . . . . .	33
<b>6</b>	<b>DISCUSSION</b>	<b>35</b>
6.1	Current study . . . . .	35

	7
6.2 Future work . . . . .	35
<b>7 CONCLUSION</b>	<b>36</b>
<b>REFERENCES</b>	<b>37</b>

# 1 INTRODUCTION

## 1.1 Background

Optical fiber is a key component of communication technology, representing a remarkable technical revolution in recent telecom history [1]. Undoubtedly, the invention of optical fibers was one of the most important technological advancements in data communications. They have gradually replaced copper wire and satellite connections due to their numerous advantages, including high data speeds, minimal attenuation, and resistance to electromagnetic interference [2, 3]. Besides telecom purposes, fibers are also used in the non-telecommunications domain. They are widely applied for illumination, remote sensing, machining, medical imaging, and linking applications, thanks to their compact size, lightweight, large bandwidth, and other desirable properties [4]. A conventional optical fiber (Fig. 1) [5] is made of two silica ( $\text{SiO}_2$ ) glasses – an advanced refractive index (RI) core and a lower RI cladding. The higher RI core is typically obtained by doping the silica with either fluorine (F) or germanium (Ge) atoms [6]. Such a fiber guides light through total internal reflection (TIR) [7]. While optical fibers enable widespread applications, conventional fibers have inherent limitations due to the properties of the glass used in their composition [8].

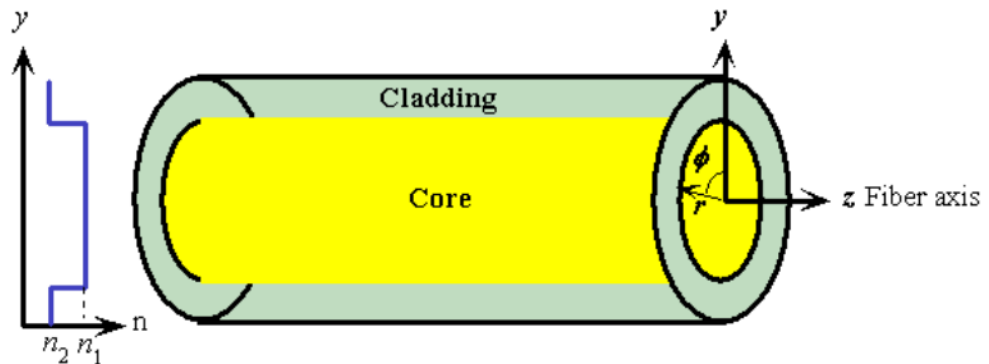


**Figure 1.** Conventional optical fiber [5].

The properties of ( $\text{SiO}_2$ ) glass do not meet the requirements for precise emerging implementations, thus traditional fibers are unable to accommodate them. The difficulty associated with conventional fibers has sparked a latent development in fiber optics advancement, leading to the innovation of the photonic crystal fiber (PCF), also known as the holey optical fiber (HOF) or the microstructure optical fiber (MOF) [9]. In 1987, the

photonic band gap (PBG), initially proposed by Sajeev John of the University of Toronto and Eli Yablonovitch from Bell Communications Research, gained significant attention in optics during the early 1990s [10]. The PBG involves constructing structures to hinder the conveyance of photons at specific wavelengths while allowing passage at others. Furthermore, minor alterations in the regularity of the RI would commence additional power levels amidst the PBG, akin to the generation of energy levels amidst the band gap of traditional semiconductors. Regrettably, crafting the appropriate compositions has proven to be exceedingly challenging. The inaugural PBG substance was crafted in 1991 by Yablonovitch and his collaborators through the process of drilling cavities with 1 mm dimensions in a material block possessing an RI of 3.6. Given that the band gap wavelength aligns with the interval between the air apertures in the crystalline, this configuration exhibited a bandgap inside the warm zone.

Inspired by Yablonovitch's research, Philip Russell proposed in 1991 a groundbreaking idea to confine light within a hollowed core fiber by introducing a two-dimensional (2-D) optical crystal in the cladding—a cyclic lattice of tiny air apertures within glass [11]. This concept draws on the same principle found in the iridescence of peacock feathers or butterfly wings, where periodic nanostructures produce various angles and colors, creating stop bands that strongly reflect inward light. When skillfully formulated, the photonic crystalline cladding proceeding alongside the overall fiber size can avert the escaping of illumination from the core. These novel fibers are named PCFs as they bank on the unfamiliar attributes of photonic crystalline.

The crystal lattice of silica is highly transparent and has some prominent optical properties. Relying upon these exclusive properties optical fiber is made. In recent years, there has been active research on advancing optical fiber and PCF technology [11–14]. A modern class of optical fiber PCF, a modern form of optical fiber, is constructed with a simulated array of air apertures running longitudinally through the fiber, offering superior performance compared to standard fibers. PCF offers magnificent optical features like endless single-mode operation, large effective area, ultra-flattened dispersion, high nonlinearity, and high birefringence (Br), as distinctly reported in previous literature [12]. These crucial properties largely depend on PCF size or shape, light propagating mechanism, hosting material, and operating wavelength. These are reported below. Light propagation through PCF is classified into two classes: PBG and index guiding (IG) (in Fig. 2) [13]. In IG-PCF, light travels through the fiber core where the RI is greater than the cladding region, leading to TIR phenomena. In contrast, PBG-PCF utilizes a photonic band gap effect to instruct light through the fiber core. PBG-PCF typically has a narrower transmission band compared to IG-PCF [14]. While conventional optical fiber is typically

made of doped silica, for PCF its conventional optical properties are not sufficient [15]. Various materials such as tellurite, chalcogenide, and graphene glass with polymer are used as backgrounds to form PCF, especially over larger infrared transmission bands, due to their novel optical properties [16].

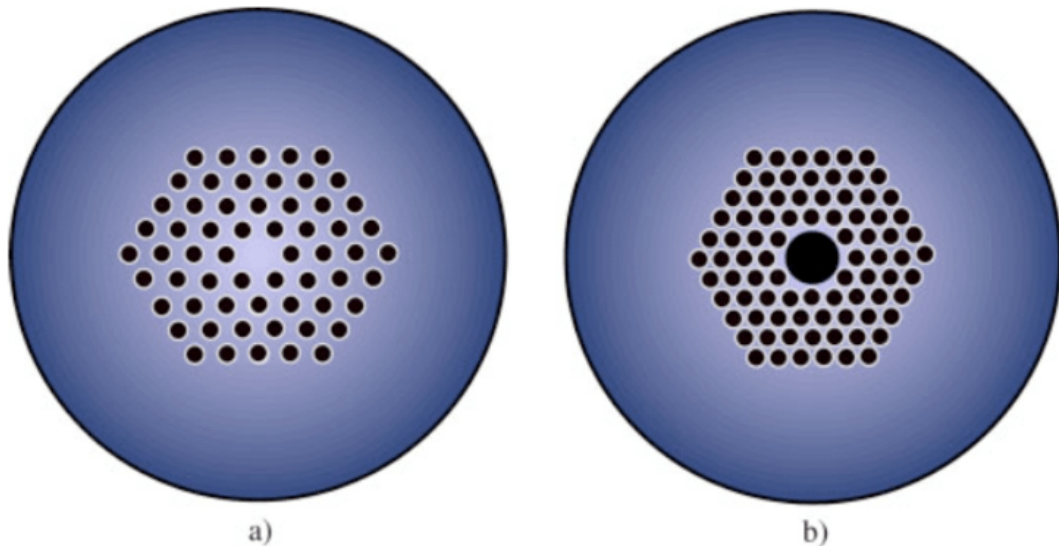


**Figure 2.** Structure of index guiding (a) and photonic band gap (b) PCF [13].

Application areas of PCF are growing vigorously. In the field of telecommunication, it opened a new era for fast communication. The internet backbone is based on optical fiber. Besides telecom sectors, PCFs are used in the areas of sensing (chemical, gas pressure, temperature), biological diagnostics, optical coherence tomography (OCT), spectroscopy, high-power technology, optical switching, optical amplification, supercontinuum generation, optical filtering, and so forth [17, 18]. Recently PCF has drawn great attention by filtering the light for faster communication [14]. A miraculous change has already been made in neuroscience by imaging the brain system [11, 12].

## 1.2 Objectives and delimitations

The objectives of this thesis are as follows:

- Develop a novel optical waveguide structure known as SS-PCF.
- Attain improved nonlinear characteristics while ensuring a straightforward and flexible design.

- Use FEM with a fine mesh to analyze and evaluate key optical properties.
- Evaluate the performance of different core materials, such as GaP, graphene, and tellurite, separately in the SS-PCF structure.
- Discuss potential fabrication methods for the proposed SS-PCF, considering techniques such as sol-gel and capillary stacking for efficient manufacturing.
- Propose avenues for future research based on the potential applications and advantages of the designed SS-PCF structure.

The delimitation of this thesis work is that the fiber properties are computed only within a limited wavelength range from  $0.1 \mu\text{m}$  to  $1.5 \mu\text{m}$ .

### **1.3 Structure of the thesis**

Chapter 2 provides an extensive overview of PCF and its guiding mechanism. It also discusses the role of nonlinear PCF in supercontinuum generation and various nonlinear optical phenomena. Chapter 3 presents the geometric features of the proposed PCF structure with its core materials. It delves into the simulation criteria and numerical techniques that are utilized for analyzing the optical characteristics focusing on the FEM as a primary approach, and also the fabrication techniques like capillary stacking, sol-gel, drilling, and 3D printing. Chapter 4 outlines the several optical parameters that are computed to provide a comprehensive understanding and potential applications of SS-PCF. Chapter 5 is related to graphical descriptions of all the calculated parameters with three different materials. Chapter 6 represents the current study and future work. Chapter 7 encompasses conclusions.

## 2 PRINCIPLES OF PHOTONIC CRYSTAL FIBERS

### 2.1 Literature Review

The exploration of PCF has gained immense popularity due to its wide range of optical applications [1, 19]. PCF guiding mechanisms can be sorted into two kinds: IG-PCF and PBG fiber. IG-PCF comprises a cyclic structure of air apertures inside the cladding segment, which traps light within the central zone and allows for the interface of light power with air or fluids inside the cladding apertures with a gradual field [20]. In PBG fiber, light is controlled through PCF in a minor-index core section [21, 22], effectively managing the guidance of light across various frequency bands. PCF has the potential to serve as electro-optical modulators [23], switches [24], filters [25], gas sensors [26–31], and fluid or chemical sensors [32], etc. PCFs exhibit good guiding characteristics and design flexibility in varying effective areas, making them attractive for optical filtering and sensing. Furthermore, the high filtering characteristics, reduced size, sensitivity, and multiplexing capability of PCFs offer potential in various applications. The design flexibility and advantages over conventional optical PCFs have drawn the attention of researchers in the modern world. Researchers have been striving to achieve superior guiding attributes of PCF by analyzing the geometrical properties in both core and cladding. Since the first invention of PCF, attaining improved guiding properties of PCF has been a great challenge for researchers. Compared to traditional optical fibers, PCFs have been shown to have better sensitivity, adjustable dispersion, high optical nonlinearity, large Br, and low confinement loss (CL) [11, 33, 34]. These distinctive features have found extensive applications across various domains, including chemistry, medicine, and biology, owing to their convenient properties [35]. When light propagates through a PCF in the presence of a metallic layer, the independent electrons within the metal absorb the optical influence of the light, leading to optical signal interaction with surface Plasmon resonance (SPR). SPR arises when their segments are identical [36]. The combination of PCF and nanoplasmonics represents a promising exploration area.

There are several publications available that discuss strategies to maximize PCF performance [37–43]. Key features and applications of the optical fiber are listed in Table 1 [44]. Researchers have explored enhancing PCF conductivity by creating a nanostructured core with a high RI to achieve large nonlinearity and Br. To accomplish high Br and nonlinearity, Liu et al. proposed an elliptical core PCF packed with tellurite glass [37]. Their research yielded Br and nonlinearity measurements at wavelengths of  $1.55 \mu\text{m}$  that were successively  $7.57 \times 10^{-2}$  and  $188.39 \text{ W}^{-1}\text{km}^{-1}$ . Wang et al. created

**Table 1.** Types of Optical Fibers, Key Features, Applications, and Examples [44].

Types	Key Features	Applications	Examples
Multi-mode	Transmit multiple signals over limited distances	Signal transmission, local area networks, video distribution, lighting systems	Multi-mode fibers
Single-mode	Transmit multiple signals over large distances	Submarine communications, high speed data transfer, long-haul telecom networks	Single-mode fibers
Rare-earth-doped	Wavelength selectivity, long lifetime, broadband amplification	Nonlinear optics, quantum optics, telecoms networks, cryptography	Rare-earth-doped fibers
Air clad	Ultra-high NA, multi-mode, pure silica core	Spectroscopy, Power delivery	Air clad fibers
Hollow core	Low latency, minimal dispersion, elevated distraction threshold	Distribution of ultra-short high energy optical pulses, pulse compression, ultra-fast data transmission, pulse shaping	hollow core fibers
PCF	High nonlinearity, low-loss transmission, high birefringence, broad continuous operational spectrum	Telecommunications, biomedical imaging, mode filtering, sensing, short pulse delivery	Hollow core PCFs, single mode PCFs, PM PCFs

a tellurite-anchored PCF [38] in a different study that shows Br and nonlinearity up to  $5.05 \times 10^{-2}$  and  $1896 \text{ W}^{-1}\text{km}^{-1}$  consecutively, at the active wavelength of  $1.55 \mu\text{m}$ . Revathi et al. [39] however, suggested a spiral shape with elliptic air apertures and achieved Br of  $2.56 \times 10^{-2}$ . Subsequently, it was modified to  $2.96 \times 10^{-2}$  by substituting soft glass as the PCF's basic material [45]. Therefore, Yang et al. [40] suggested a PCF with condensed air apertures in the core area and offered excellent performing profiles, including strong nonlinearity of  $68 \text{ W}^{-1}\text{km}^{-1}$ , Br of  $2.22 \times 10^{-2}$ , and CL of  $10^{-4} \text{ dBm}^{-1}$ . Additionally, Liao et al. [46] described a nonlinear slot silicon fiber with a great Br of  $2.1 \times 10^{-2}$ , a nonlinearity of  $156.74 \text{ W}^{-1}\text{km}^{-1}$ , and a bigger effective area (EA) of  $1.48 \times 10^{-12} \text{ m}^2$ . At the wavelength of  $0.5 \mu\text{m}$ , Paul et al. [41] reported a high nonlinearity of  $1.52 \times 10^5 \text{ W}^{-1}\text{km}^{-1}$  with a numerical aperture (NA) of 0.36 and CL of  $1.47 \times 10^{-5} \text{ dB/m}$ . Moreover, Biswas et al. [42] evaluated D-shaped PCF with a small mode area of  $1.20 \times 10^{-13} \text{ m}^2$  and very high nonlinearity of  $5.2 \times 10^7 \text{ W}^{-1}\text{km}^{-1}$  at  $0.1 \mu\text{m}$  wavelength. Furthermore, Ahmed et al. [43] addressed a D-shaped design with Br of 0.17 and an outstanding high NA of 0.80.

## 2.2 Light Capturing Operation of Photonic Crystal Fiber

The transmission of the optical field through the fiber center is facilitated by upholding two distinct ideologies of light, namely TIR and PBG theory.

### 2.2.1 Total Internal Reflection

The fundamental concept of TIR shown in Fig. 3 [5] involves a 2-D photonic lattice, where the core material possesses a higher RI than the cladding [33]. This type of PCF consists of a solid silica core besieged by a photonic lattice featuring a triangular arrangement of air apertures [47]. The guidance of light in this PCF occurs through a modified form of TIR, known as IG-PCFs [48]. In solid core PCFs, the core is built of uncontaminated silica, while the cladding comprises multiple air apertures, increasing the disparity in RI betwixt the core and the cladding. This difference alters the light path using the principle of modified TIR.

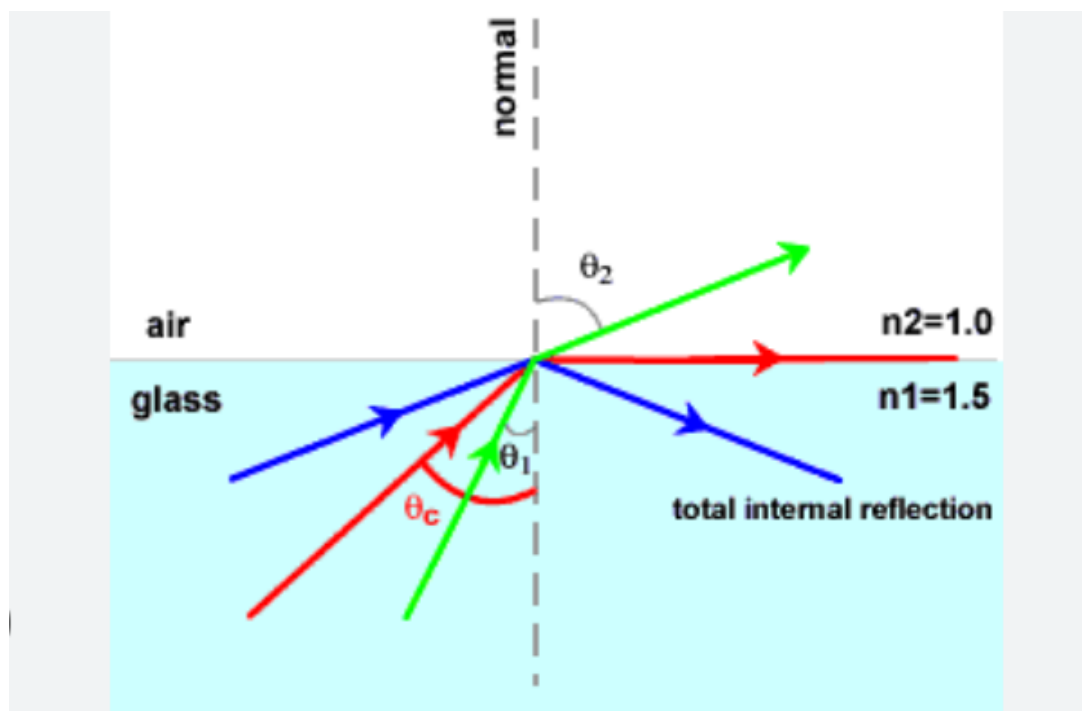


**Figure 3.** Working process of total internal reflection [5].

### 2.2.2 Photonic Bandgap Guiding

In PBG fibers (Fig. 4) [5], the RI of the cladding region exceeds that of the core area due to the presence of the hollow core [33]. Consequently, light is guided through the existence of the band gap. The fiber selectively permits photons with a band gap exceeding that of the PCF cladding [47]. Therefore, all photons with a band higher than the PCF bandgap either become evanescent in the cladding or continue propagating within the air core.

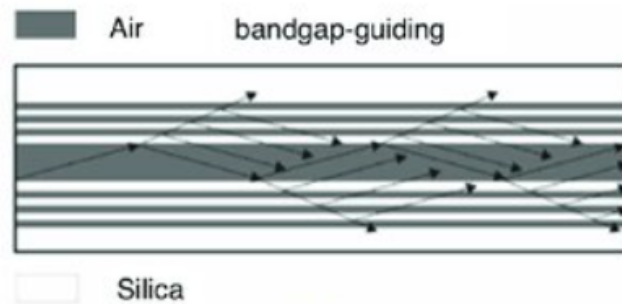


**Figure 4.** photonic bandgap guiding [5].

### 2.3 Nonlinear Photonic Crystal Fiber in Supercontinuum Generation

Nonlinear PCFs have become pivotal in the realm of supercontinuum generation, presenting distinct advantages for achieving broad optical spectra (Fig. 5) [49]. The enhanced nonlinearity of PCFs is a result of carefully crafted designs and specialized materials, allowing for efficient nonlinear optical processes like self-phase modulation (SPM), four-wave mixing (FWM), and stimulated Raman scattering. These nonlinear phenomena collectively contribute to the significant spectral broadening observed in supercontinuum generation, enabling the creation of a wide range of wavelengths from a single optical source. The controlled dispersion and unique waveguide properties of nonlinear PCFs, as well as their ability to support soliton dynamics, perform a crucial role in shaping the characteristics of the generated supercontinuum. Noteworthy references supporting the use of nonlinear PCFs for supercontinuum generation include works by [33, 47, 50], emphasizing their impact on diverse applications such as OCT, spectroscopy, and the generation

of ultrafast pulses. Researchers continue to explore and refine nonlinear PCF designs, contributing to advancements in supercontinuum sources with tailored spectral properties for various applications in optics and photonics.

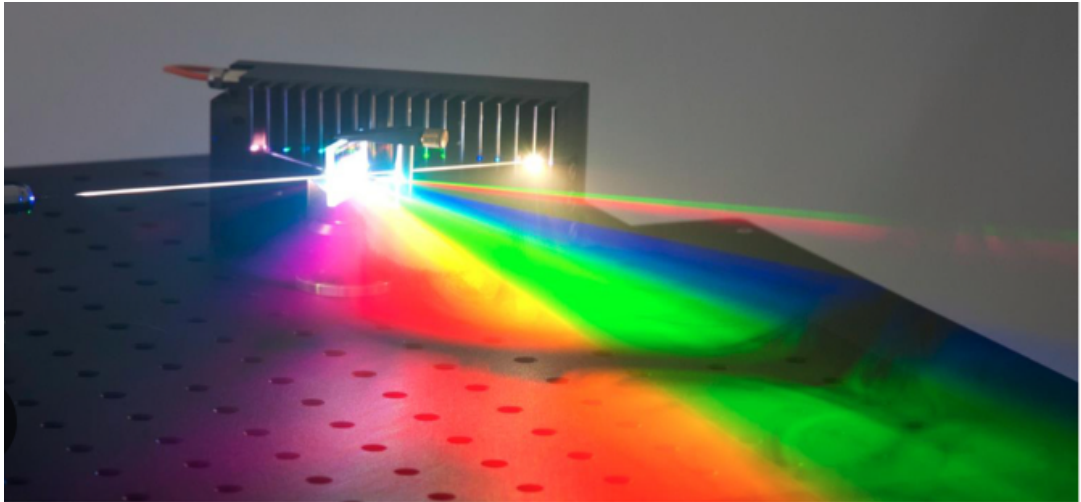


**Figure 5.** Supercontinuum generation [49].

## 2.4 Nonlinear Optical Fiber in Four-Wave Mixing

Nonlinear optical fibers (NOF) have an important role in the applications of FWM phenomena, which include, in general, most of the third-order nonlinear optical processes. These processes have a pivotal role in various applications in optical communications and signal processing. For example, the intensity-dependent RI arises from the so-called degenerate FWM, which then gives birth to the nonlinear Kerr effect. In an optical fiber, the nonlinear Kerr effect enables the generation of new frequencies when short, high-intensity, laser pulses interact in the fiber. This is essential in the wavelength conversion of optical signals, which enables enhancing the flexibility and capacity of optical communication networks [51]. Okawachi and his co-workers have experimentally shown the feasibility of FWM in wavelength tuning using microstructured optical fibers [52]. Also, FWM in optical fibers offers a foundation for the development of new photonic devices [51].

## 2.5 Nonlinear Optical Fiber in Self-phase Modulation

SPM arises when a high-intensity laser pulse propagates through a NOF and alters the pulse's temporal phase due to the fiber's optical nonlinearity, leading to the intensity-dependence of the fiber's RI. Thereby, when the pulse travels through the fiber, its leading edge experiences a higher RI than the trailing edge and creates a time-dependent phase shift. A fast temporal modulation of phase results in spectral broadening of the laser pulses (Fig. 6) [53]. Hence, SPM has an important role in supercontinuum generation, where ultra-short and high-intensity laser pulses transform into a very broad spectrum of light [54]. This phenomenon has practical applications in optical communications, spectroscopy, and laser sources for biomedical imaging. Therefore, there is a strong desire to discover new fiber designs and pulse-shaping techniques to optimize and control SPM for specific photonic applications [11].

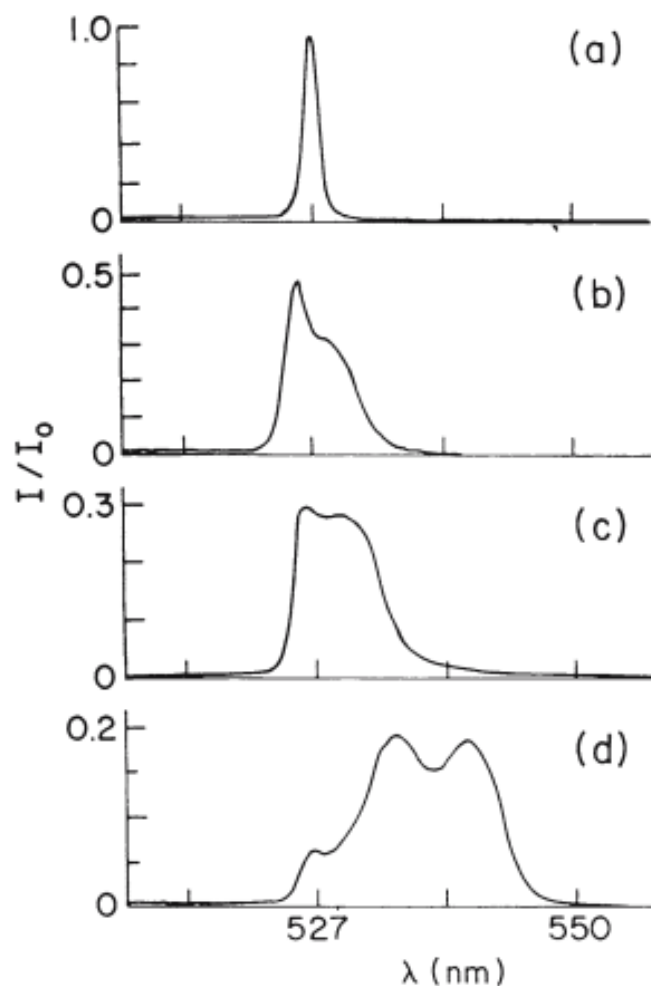


**Figure 6.** Spectral broadening due to SPM of 8 ps laser pulses at 527 nm after propagation of different lengths in an optical fiber: (a) 0 cm; (b) 22 cm; (c) 42 cm; (d) 84 cm. [53].

## 2.6 Advantages of Photonic Crystal Fiber in Nonlinear Applications

PCF presents distinctive advantages for nonlinear applications in optics. The high nonlinearity of PCFs facilitates efficient light-matter interactions, crucial for phenomena like supercontinuum generation and FWM [33,52]. The tailored dispersion properties of PCFs allow precise control over group velocity dispersion, enabling manipulation of pulse propagation and phase matching in nonlinear processes [50]. Additionally, the ability to control Brillouin scattering, coupled with enhanced light confinement within the core, provides opportunities for mitigating nonlinear limitations and optimizing signal quality [47]. The flexibility to tailor mode profiles, achieve low optical loss, and incorporate specialty designs makes PCFs a versatile platform, suitable for various applications in telecommunications, sensing, and integrated photonics devices. Compact and flexible in design, PCFs offer a promising avenue for advancing nonlinear optical technologies.

## 2.7 Nonlinear Optical Fiber in a Nutshell

All optical fibers have non-zero third-order nonlinear optical susceptibility, which gives rise to the intensity-dependent RI. Therefore, all optical fibers can show third-order nonlinear optical effects [51]. However, if an optical fiber is specifically designed to have an especially large value for the optical nonlinearity, it is called a nonlinear optical fiber or NOF. In these fibers, the nonlinear optical effects are especially pronounced, even in short NOFs. These effects include phenomena like SPM, FWM, parametric amplification, pulse compression (see Fig. 7) [55], and supercontinuum generation [54]. Notable materials for NOFs include PCFs, microstructured fibers, and specialty designs with high nonlinearity and tailored dispersion characteristics [33]. NOFs find applications in diverse fields, including telecommunications, where they enhance signal processing capabilities and enable wavelength conversion, as well as in sensing, imaging, and frequency generation [52].

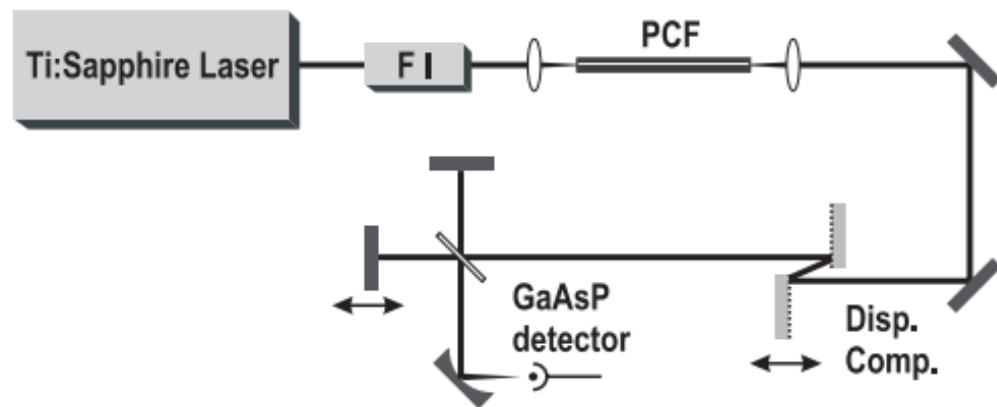


**Figure 7.** Pulse compression with PCF in practice. PCF is pumped by 250 fs laser pulses from Ti : Sapphire laser, and output pulses from PCF are spectrally broadened. These pulses are then compressed to 25 fs pulses by the negative dispersion of a grating pair [55].

### 3 DESIGN OF SPIRAL-SHAPED PHOTONIC CRYSTAL FIBER

#### 3.1 Geometry

COMSOL Multiphysics 5.1, an all-encompassing simulation package with a wide variety of application programs, was used to design the SS-PCF structure. Fig. 8 illustrates the cross-segmental outlook of the intended SS-PCF where each spiral arm has 10 air holes. In the middle position, an ellipse core is set where its  $a$  and  $b$  semi-axis values are  $0.35$  and  $0.17 \mu\text{m}$  respectively. The center area is presented in Fig. 9, and the corresponding triangular mesh used in the FEM computations is shown in Fig. 10. Here,  $d_1$  to  $d_3$  are the diameter of cladding air apertures, and their values are  $0.96$ ,  $1.26$ , and  $2 \mu\text{m}$  correspondingly. Furthermore, we have set a radius of  $13.75 \mu\text{m}$  for the perfectly matched layer-1 (PML1) and  $12.5 \mu\text{m}$  for PML2, with its thickness being 10% of the total PCF. The spacing between the centers of two adjacent apertures is called the pitch distance ( $P$ ). For the core material, GaP, tellurite, and graphene are separately employed, while silica acts as the framework material. Fig. 11 depicts the mode field distribution across two different wavelengths  $0.1 \mu\text{m}$  and  $1 \mu\text{m}$ , with a specific focus on both X and Y polarizations.

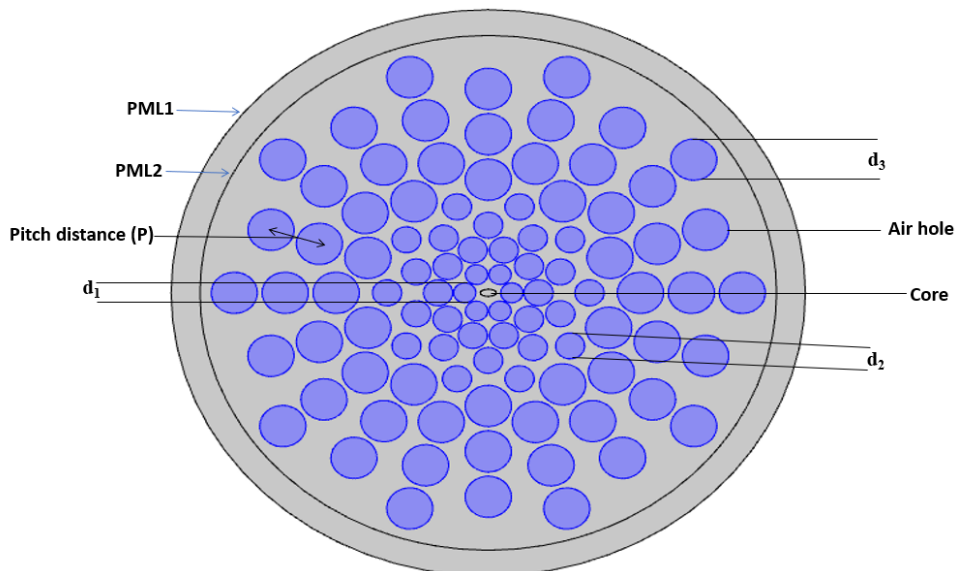


**Figure 8.** The cross-segmental outlook of the proposed SS-PCF.

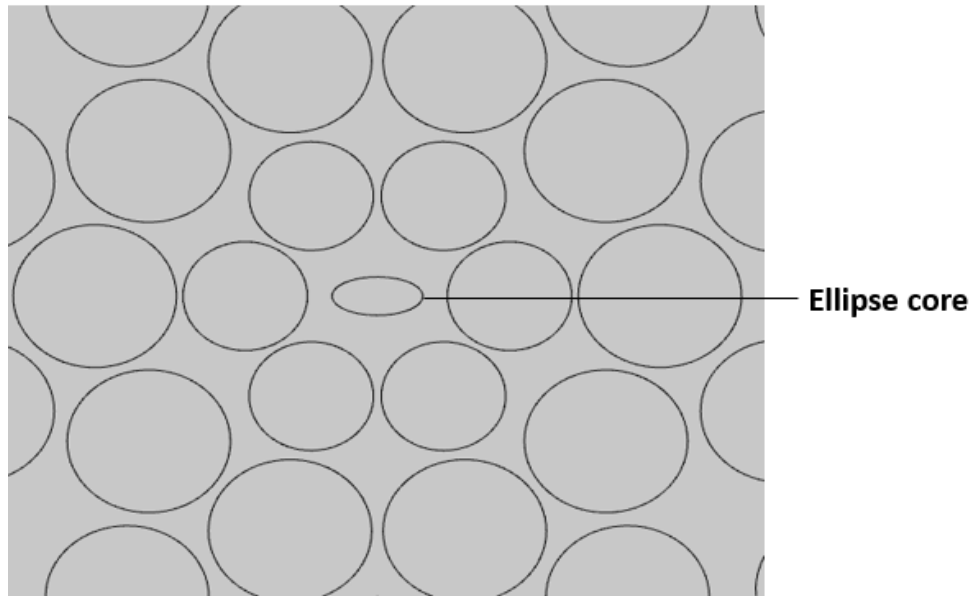


**Figure 9.** Closer look of the center area.

### 3.2 Simulation Criteria

For analyzing optical characteristics, various numerical techniques such as finite difference time domain (FDTD), partial wave expansion (PWE), effective mode index (EMI), and full vector finite element method (FV-FEM) are well known [56–59]. Of these techniques, FV-FEM is the best technique for its less computational time [60]. Additionally, mesh analysis also plays a crucial role, as being responsible for the complete discretization of the designed prototype into easy shapes [61]. In this thesis work, FV-FEM has been applied for searching the propagating modes, and the comprehensive vectorial program COMSOL Multiphysics 5.1 was used to complete the entire analysis.

### 3.3 Finite Element Method

In many fields of physics and engineering, some phenomena or systems can be described by partial differential equations (PDEs) [59–61]. For complicated systems, these equations are unsolvable in practice. To solve this problem, an American-German mathematician, Richard Courant, developed the finite element method (FEM) in 1940 [62]. The fundamental concept of FEM involves dividing the computation domain into small subdomains that are known as finite elements. This is accomplished through a specific discretization of space dimensions, implemented by creating a mesh of objects. This mesh serves as the numerical domain for the solution, containing a finite set of points [63]. The

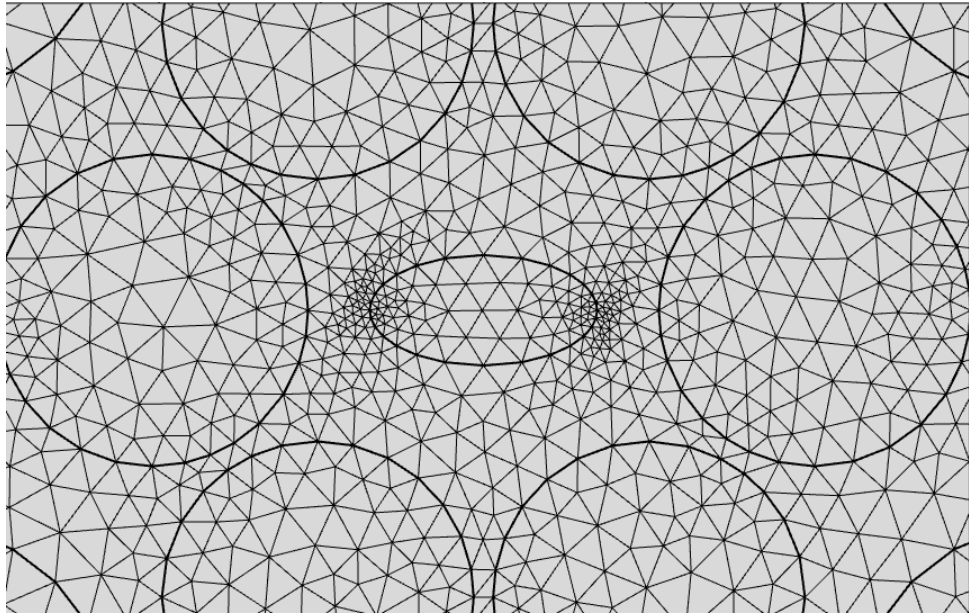


**Figure 10.** Triangular mesh of the proposed SS-PCF structure.

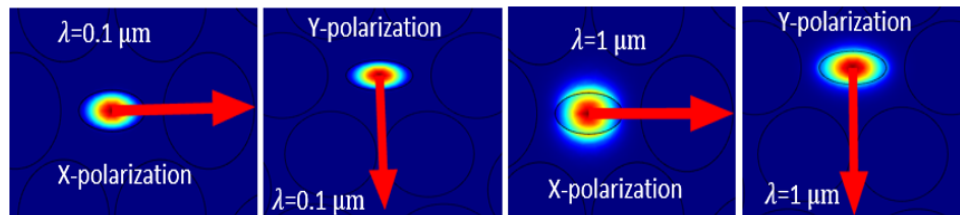


**Figure 11.** X and Y polarization mode distribution at two different wavelengths.

PDEs are then solved for each subdomain using suitable boundary conditions. 2-D and 3-D finite elements are extensively used for their variable mesh and curve structures. An example of the FEM technique applied to a PCF structure is shown in Fig. 12 [64].

### 3.4 Fabrication Process

The fabrication process is a critical aspect to consider when it comes to PCFs. In this context, extensive research has been conducted to determine the feasibility of fabricating the designed PCF. Additionally, various fabrication methods, including extrusion, stack-and-draw [65], capillary stacking, sol-gel [66], drilling, and 3D printing, have been comprehensively discussed in the study. In a recent laboratory experiment, Jabin et al. successfully manufactured a PCF with an amoeba-shaped configuration [67], which presents a more challenging structure compared to my design. Furthermore, using the conventional capillary stacking technique, Argyros et al. created a micro-structured polymer fiber adorned with circular rings of perforations [68]. The proposed SS-PCF can be effi-

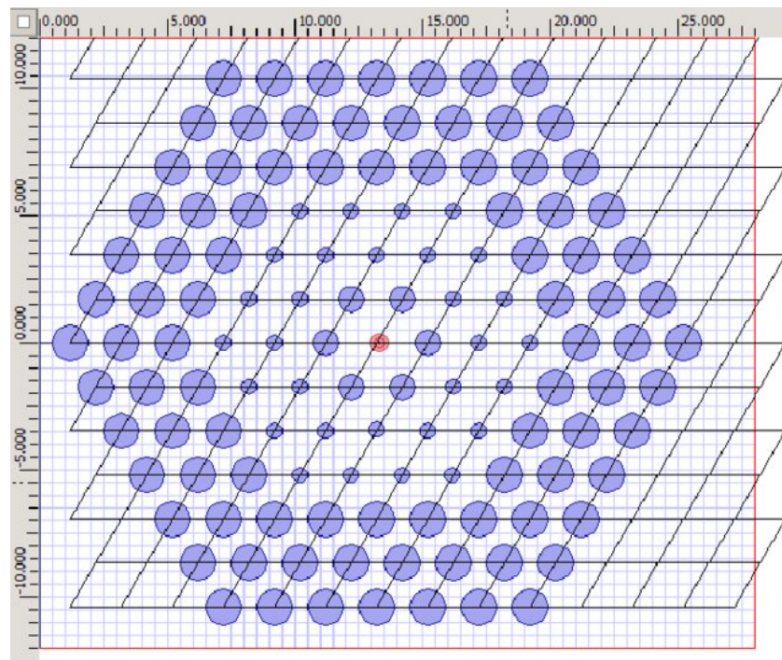


**Figure 12.** A PCF structure using FEM technique [64].

ciently manufactured through the utilization of sol-gel and capillary stacking techniques. These methods can provide the necessary additional structural flexibility for the envisioned design.

## 4 NUMERICAL CHARACTERIZATION

### 4.1 Refractive Index

In PCFs, the refractive index (RI) or index of refraction represents a dimensionless parameter that describes how light transmits through a medium. Based on its performance profile, a unique SS-PCF is presented in this thesis work. The comprehensive vectorial program COMSOL Multiphysics 5.1 was used to complete the entire analysis. Analysis of the 235 430 mesh elements is aided by FEM. The whole evanescent field is assessed by two different forms of mode confinement, namely x-polarization and y-polarization. Furthermore, the mesh findings are mostly used for the core material, indicating the structure's effective RI, which can be calculated as [69]

$$n(\lambda) = \sqrt{1 + \sum_{i=1}^3 \left[ \frac{B_i \lambda^2}{\lambda^2 - C_i} \right]}, \quad (1)$$

where  $B_i$  and  $C_i$  are Sellmeier constants, and  $n$  implies the RI of fused silica that varies on wavelength. The standard temperature in this area is 25 °C.

### 4.2 Birefringence

Birefringence refers to the optical characteristic where RI varies based on polarization and direction of light propagation. However, it is possible to determine the modal birefringence, which is defined as the differentiation of the orthogonal mode RI difference [69, 70]:

$$Br(\lambda) = |n_x - n_y|, \quad (2)$$

where  $n_x$  and  $n_y$ , respectively, are the effective mode RI of the core material in x and y polarization.

### 4.3 Beat Length

The beat length ( $L_b$ ) of a PCF can be used to gauge its polarization-preserving capabilities. It is reliant on the operating wavelength and Br. The subsequent formula can be applied to calculate the PCF's beat length and is given by [43]:

$$L_b = \frac{Br}{\lambda}. \quad (3)$$

### 4.4 Power Fraction

The principal goal of the suggested PCF is to dispatch information utilizing output power. Consequently, power fraction acts as an indicator of the fiber's overall performance and is given by [71]:

$$\eta = \frac{\int_x S_z dA}{\int_{\text{all}} S_z dA}. \quad (4)$$

Here, the numerator signifies the current region of interest, while the denominator denotes the entire region of interest, and  $S_z$  is a Poynting vector that describes the z-direction of wave transmission.

### 4.5 Confinement Loss

Confinement loss (CL) occurs when the guided light extends into the cladding region, and the light leaking through the air holes within the cladding is called leakage loss or CL. Therefore, electromagnetic wave leakage and absorption cause the power decline at the output, which is revealed by the confinement loss, and its equation is given by [43]:

$$L_c = \frac{20}{\ln 10} \times \frac{2\pi}{\lambda} \times \text{Im}(n_{\text{eff}}) \times 10^{-2}, \quad (5)$$

where  $\text{Im}(n_{\text{eff}})$  and  $\lambda$  stand for the imaginary values of the RI and wavelength, respectively.

## 4.6 Effective Mode Area

The effective mode area ( $A_{\text{eff}}$ ) refers to the spatial distribution of a light beam within a fiber. Calculating  $A_{\text{eff}}$  is crucial as it provides valuable insight for estimating several parameters like NA and nonlinearity. Conversely, the total polarization profile, shown by  $A_{\text{eff}}$ , is fully dependent on the region of mode confinement given by [72]:

$$A_{\text{eff}} = \frac{\left( \int \int |E(x, y)|^2 dx dy \right)^2}{\int \int |E(x, y)|^4 dx dy}, \quad (6)$$

where  $E(x, y)$  is the electric field amplitude. The integration process involves the entire area, not just the core region.

## 4.7 Numerical Aperture

In optics, numerical aperture represents a dimensionless value that defines the breadth of angles within which the mechanism can emit or accept light [73]. On the other hand, the receiver's ability to take all light is entirely dependent on the SS-PCF's numerical aperture given as [71]:

$$\text{NA} = \left[ \sqrt{1 + \frac{\pi A_{\text{eff}}}{\lambda^2}} \right]^{-1}. \quad (7)$$

## 4.8 Nonlinearity

The high nonlinear PCF is well-suited for practical applications. The effective mode field and nonlinear coefficient influence a fiber's nonlinearity. Higher nonlinearity ( $\gamma$ ) is produced by a small effective area ( $A_{\text{eff}}$ ) and a big nonlinear coefficient ( $n_2$ ), and vice versa. The nonlinearity ( $\gamma$ ) of a PCF can be evaluated by [74]:

$$\gamma = \frac{2\pi}{\lambda} \times \frac{n_2}{A_{\text{eff}}}. \quad (8)$$

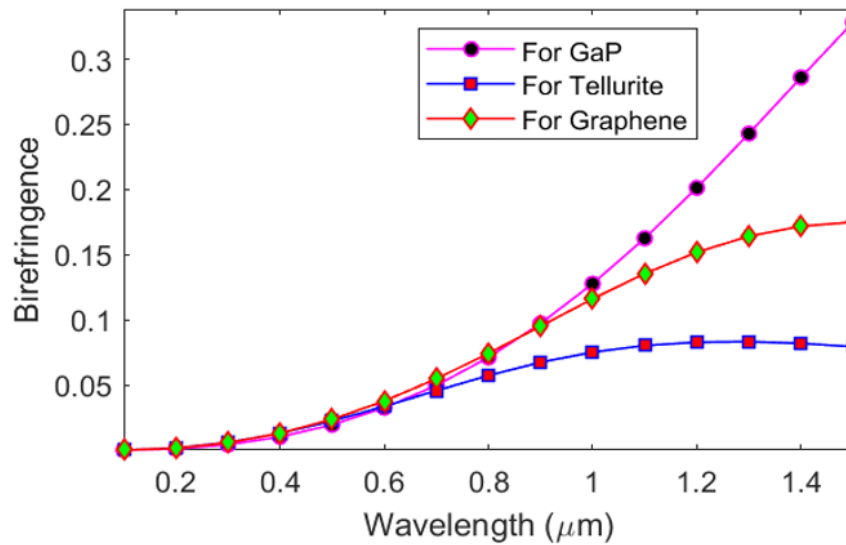
Here,  $A_{\text{eff}}$  stands for the effective area, while  $n_2$  for the core material's nonlinear coeffi-

cient.

## 5 RESULTS

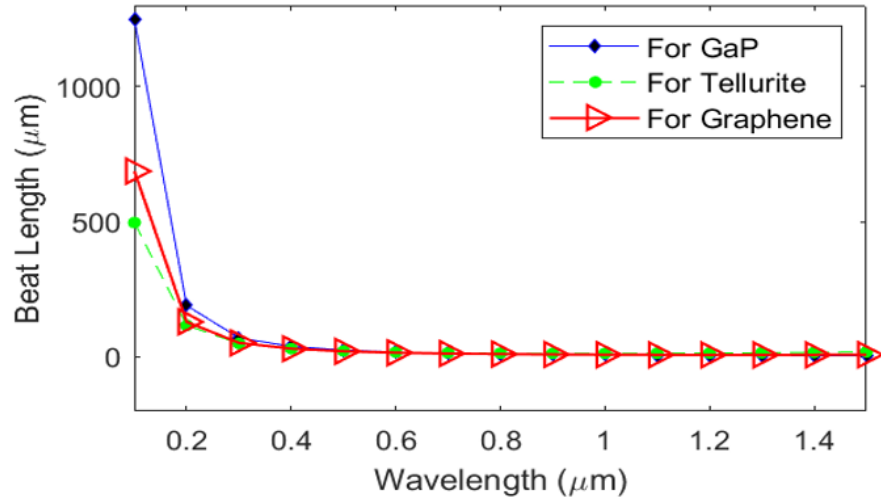
### 5.1 Simulation Results of the Proposed Optical Fiber Structure

The effective wavelength modification of modal Br of GaP, graphene, and tellurite is illustrated in Fig. 13. The Br increases with increasing wavelength. In the wavelength range from 0.1 to 0.7  $\mu\text{m}$ , each material has almost the same Br. In wavelengths between 0.7 to 1.5  $\mu\text{m}$ , the materials show different Br curves, GaP showing the maximum Br value of 0.33 at a wavelength 1.5  $\mu\text{m}$ . It is important to note that many applications utilize materials with strong Br. For instance, it is crucial in long-distance communication as well as in lowering the PMD impact. Consequently, the very high Br value of the designed SS-PCF is one of its advantages over conventional PCFs.



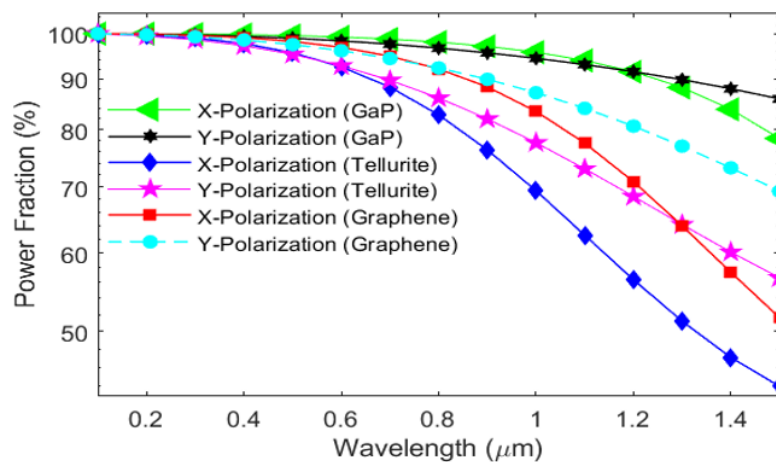
**Figure 13.** The behavior of birefringence with respect to the wavelength for GaP, tellurite, and graphene.

The PCF's ability to preserve polarization can be assessed by beat length ( $L_b$ ). Fig. 14 exposes the  $L_b$  and it is getting shorter as the wavelength increases. The highest  $L_b$  is achieved at 0.1  $\mu\text{m}$  wavelength for all materials. For this wavelength GaP, tellurite, and graphene have maximum  $L_b$  values of 1247.48  $\mu\text{m}$ , 496.94  $\mu\text{m}$  and 687.26  $\mu\text{m}$  respectively. At operating wavelengths from 0.4  $\mu\text{m}$  to 1.5  $\mu\text{m}$ , the beat lengths are almost the same for all materials. A PCF with a short beat length is greatly desired for optical applications that retain polarization.



**Figure 14.** Beat length graph regarding performing wavelength for GaP, tellurite, and graphene.

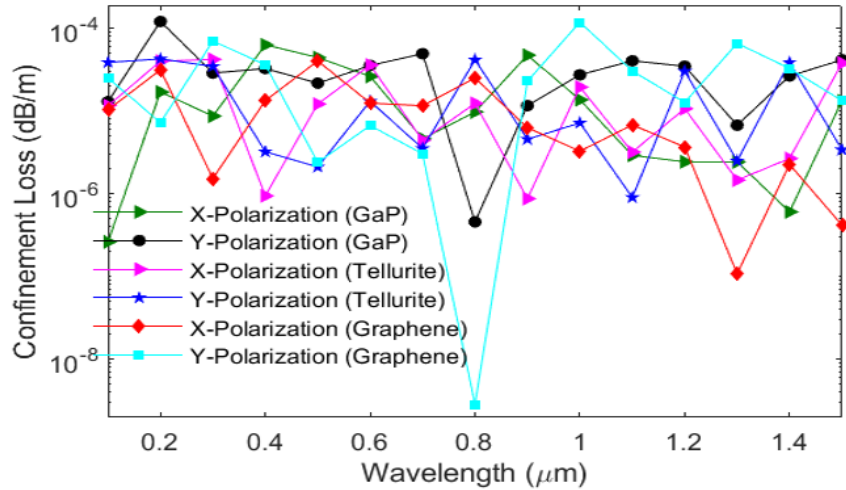
In Fig. 15, it is shown that the core power fraction decreases both in x and y polarization modes as wavelength increases, indicating that the light leaves the core area as the wavelength increases. The greatest power fraction is attained at  $0.1 \mu\text{m}$  wavelength. GaP, tellurite, and graphene, in that order, have the largest power fraction values (in percent) at this wavelength, which are 99.998, 99.989, and 99.995, respectively. The power fraction grows monotonically as the wavelength decreases. This phenomenon decreases nonlinearity (details in Fig. 19) and raises confinement loss (details in Fig. 16).



**Figure 15.** For the proposed configuration in both polarizations, the power fraction profile and wavelength for GaP, tellurite, and graphene.

In relation to wavelength fluctuations for the materials GaP, tellurite, and graphene, confinement loss ( $L_c$ ) is depicted in Fig. 16. Here, we can see the  $L_c$  of these three core

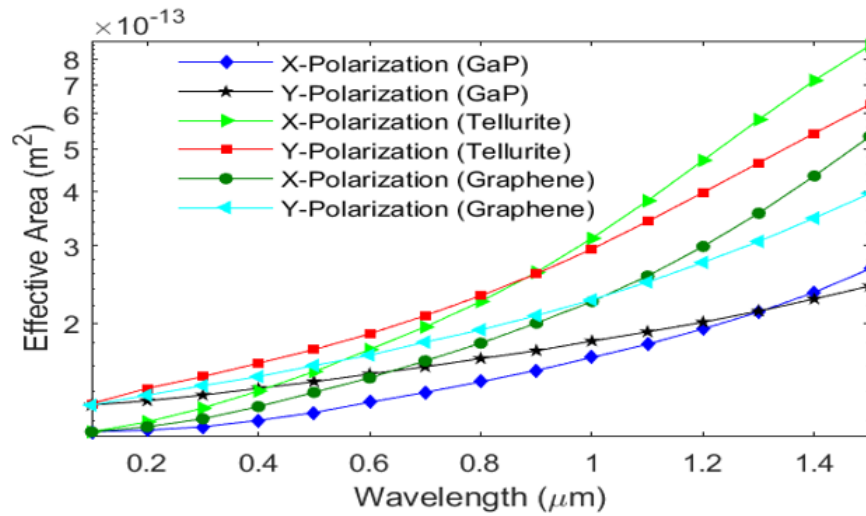
materials remain within a constant range like  $10^{-4}$  dBm $^{-1}$  to  $10^{-6}$  dBm $^{-1}$  for both X and Y-modes. Graphene shows its lowest  $L_c$  of  $2.86 \times 10^{-9}$  dBm $^{-1}$  at an operating wavelength  $0.8 \mu\text{m}$  because at this position the power fraction value is maximum. The suggested model with low  $L_c$  performance stimulates further investigation of optical factors. As a result, this SS-PCF will be compatible for long-distance contact systems.



**Figure 16.** The confinement loss for GaP, tellurite, and graphene materials regarding wavelength change in x, y polarization modes.

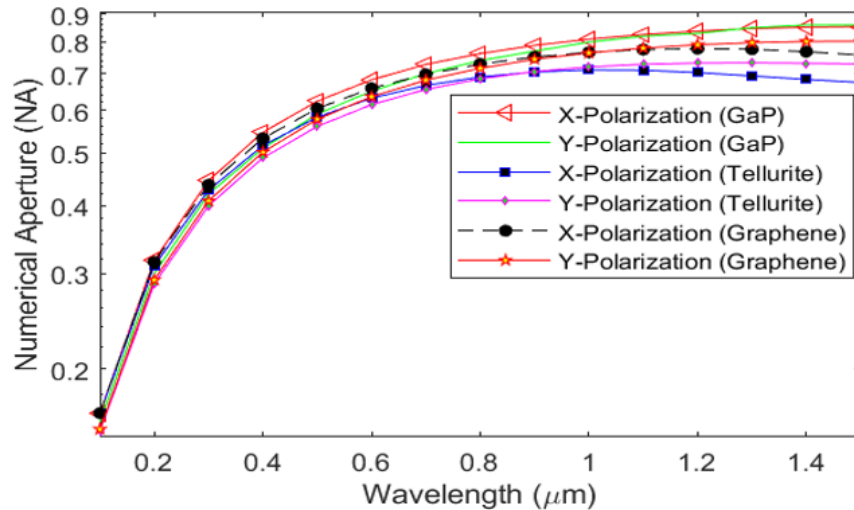
In Fig. 17, a smooth upward-sloping curve is shown for X and Y polarization of an effective mode region for GaP, tellurite, and graphene. At wavelength  $0.1 \mu\text{m}$  the values of  $A_{\text{eff}}$  is  $1.13 \times 10^{-13}$  for all three core materials in the x-polarization mode. Tellurite displays a huge effective area while GaP displays a small one. When the wavelength increases, the  $A_{\text{eff}}$  also increases. Additionally, the compact  $A_{\text{eff}}$  facilitates obtaining a high NA and extreme nonlinearity.

Fig. 18 illustrates the changes in NA concerning the wavelength. Additionally, it presents a consistently rising curve with a convex shape spanning from  $0.1 \mu\text{m}$  to  $1.5 \mu\text{m}$  across three distinct core materials. From this figure it is also evident that the top NA achieved are 0.86, 0.72, and 0.80 for GaP, tellurite, and graphene correspondingly when operating at a wavelength of  $1.5 \mu\text{m}$ . Nevertheless, it is important to note that the proposed SS-PCF structure demonstrates an NA exceeding 0.86, making it highly comparable to the previously mentioned articles [37–40, 45, 46, 75, 76]. Typically, silica rarely achieves an NA exceeding 0.40. These elevated NA values hold considerable promise for various optical applications, such as medical imaging and OCT. Therefore, the high NA values are poised to provide valuable guidance for the design of future optical fibers and will act



**Figure 17.** The effective area for GaP, tellurite, and graphene materials regarding wavelength change in the x and y polarization modes.

as a pivotal responsibility in a range of nonlinear applications.



**Figure 18.** Numerical aperture for GaP, tellurite, and graphene materials about wavelength variation in x and y polarization modes.

Fig. 19 displays a horizontal downward curve for the nonlinearity of three different materials with respect to wavelength variation. At operating wavelength  $0.1 \mu\text{m}$ , graphene shows the maximum nonlinearity, measuring  $6.13 \times 10^{12} \text{ W}^{-1}\text{km}^{-1}$  for x-polarization and  $5.31 \times 10^{12} \text{ W}^{-1}\text{km}^{-1}$  for y-polarization. Other two minerals, like GaP of  $3.70 \times 10^6 \text{ W}^{-1}\text{km}^{-1}$  and tellurite of  $3.28 \times 10^5 \text{ W}^{-1}\text{km}^{-1}$ , exhibit their maximum nonlinearity that is extremely comparable with previously reported results [41,42]. Nonlinearity has a strong

relationship with the effective area and NA which are represented in Figs. 17 and 18, respectively. The designed SS-PCF shows the highest nonlinearity achieved thus far. As a result, the suggested PCF is a promising option for telecom applications and supercontinuum production due to its high nonlinearity.

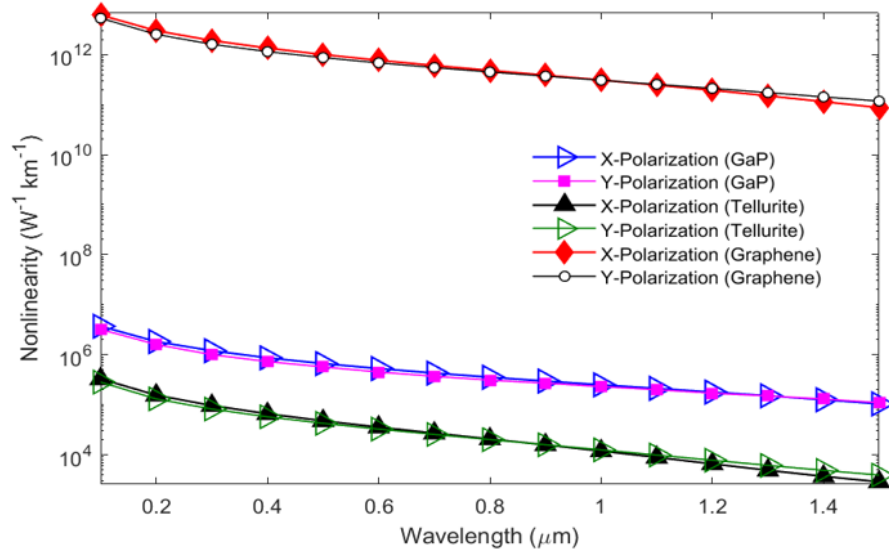


**Figure 19.** The nonlinearity diagram for materials such as GaP, tellurite, and graphene regarding wavelength variation in the x and y polarization modes.

The optical characteristics of the designed SS-PCF using different materials are shown in Table 2, and a comparison of their properties of previously reported works is shown in Table 3.

**Table 2.** Comparison of the optical characteristics of graphene, tellurite, and GaP materials for the x and y polarization modes at wavelength of  $0.1 \mu\text{m}$ . The best results are written in boldface.

Materials	Effective Mode Area ( $\text{m}^2$ )	Confinement Loss ( $\text{dBm}^{-1}$ )	NA	Nonlinearity ( $\text{W}^{-1}\text{km}^{-1}$ )
GaP (x-polarization)	$1.13 \times 10^{-13}$	<b><math>2.634 \times 10^{-7}</math></b>	<b>0.166</b>	$3.70 \times 10^6$
GaP (y-polarization)	$1.30 \times 10^{-13}$	$1.306 \times 10^{-5}$	0.160	$3.20 \times 10^6$
Tellurite (x-polarization)	$1.13 \times 10^{-13}$	$1.167 \times 10^{-5}$	<b>0.166</b>	$3.28 \times 10^5$
Tellurite (y-polarization)	$1.31 \times 10^{-13}$	$3.591 \times 10^{-5}$	0.154	$2.83 \times 10^5$
Graphene (x-polarization)	$1.13 \times 10^{-13}$	$1.040 \times 10^{-5}$	<b>0.166</b>	<b><math>6.13 \times 10^{12}</math></b>
Graphene (y-polarization)	$1.30 \times 10^{-13}$	$2.520 \times 10^{-5}$	0.155	<b><math>5.31 \times 10^{12}</math></b>

**Table 3.** Comparison of optical parameters with previous reported work and the best values are marked with boldface.

<b>Ref.</b>	<b>Wave-length (<math>\mu\text{m}</math>)</b>	<b>Birefringence</b>	<b>Power Fraction (%)</b>	<b>Confinement Loss (<math>\text{dBm}^{-1}</math>)</b>	<b>NA</b>	<b>Nonlinearity (<math>\text{W}^{-1}\text{km}^{-1}</math>)</b>
[37]	1.55	$7.57 \times 10^{-2}$	-	$2.98 \times 10^{-9}$	-	188.39
[38]	1.55	$5.05 \times 10^{-2}$	-	-	-	1896
[39]	0.85	$2.56 \times 10^{-2}$	-	-	-	26.73
[40]	1.55	$2.2 \times 10^{-2}$	-	$10^{-4}$	-	68
[41]	0.5	-	-	$1.47 \times 10^{-5}$	0.36	$1.52 \times 10^5$
[42]	0.1	-	99.99	$4.32 \times 10^{-4}$	0.86 (1.5 $\mu\text{m}$ )	$5.2 \times 10^7$
[43]	0.1	0.17 (1.5 $\mu\text{m}$ )	97	$10^{-4}$	0.80 (1.5 $\mu\text{m}$ )	-
-	0.1	$2.01 \times 10^{-4}$ (for tellurite)	99.99 (for GaP and graphene)	$2.63 \times 10^{-7}$ (for GaP)	0.166 (for GaP and graphene)	$6.13 \times 10^{12}$ (for graphene)
-	0.80	0.074 (for graphene)	98.04 (for GaP)	$2.86 \times 10^{-9}$ (for graphene)	0.76 (for GaP)	$4.80 \times 10^{11}$ (for graphene)
-	1.50	<b>0.33</b> (for GaP)	85.88 (for GaP)	$4.19 \times 10^{-7}$ (for graphene)	<b>0.86</b> (for GaP)	$1.17 \times 10^{11}$ (for graphene)

## 5.2 Summary

During this work, it was found that graphene exhibits extremely high nonlinearity of  $6.13 \times 10^{12} \text{W}^{-1}\text{km}^{-1}$  and  $5.31 \times 10^{12} \text{W}^{-1}\text{km}^{-1}$ , GaP of  $3.70 \times 10^6 \text{W}^{-1}\text{km}^{-1}$  and  $3.2 \times 10^6 \text{W}^{-1}\text{km}^{-1}$ , and tellurite of  $3.28 \times 10^5 \text{W}^{-1}\text{km}^{-1}$  and  $2.83 \times 10^5 \text{W}^{-1}\text{km}^{-1}$  for x, and y-polarized modes individually at the functioning wavelength 0.1  $\mu\text{m}$ . It also provides an ultra-high Br of 0.33, a high NA of 0.86, and a very low CL of  $2.86 \times 10^{-9} \text{dBm}^{-1}$ . At a typical laser wavelength of 0.8  $\mu\text{m}$  we can see the nonlinearity of graphene is  $4.8 \times 10^{11} \text{W}^{-1}\text{km}^{-1}$  and  $4.47 \times 10^{11} \text{W}^{-1}\text{km}^{-1}$  GaP of  $3.55 \times 10^5 \text{W}^{-1}\text{km}^{-1}$  and  $3.1 \times 10^5 \text{W}^{-1}\text{km}^{-1}$ , and tellurite of  $2.06 \times 10^4 \text{W}^{-1}\text{km}^{-1}$  and  $2.00 \times 10^4 \text{W}^{-1}\text{km}^{-1}$  for x, y-polarized modes accordingly. These values are all quite comparable to those reported in previously published articles [37–43]. These features make the suggested SS-PCF particularly suitable for various optical fields. The strong nonlinearity of the SS-PCF is very important for optical communication requirements, supercontinuum creation, spectroscopic systems, creating short pulses, polarization maintenance in optical fibers, and more. The SS-PCF's smooth and easily adaptable structure lends itself to efficient

fabrication processes. Consequently, given its exceptional performance capabilities, it is probable that the suggested SS-PCF will open new avenues for future research in the realm of PCF.

## 6 DISCUSSION

### 6.1 Current study

In this research work, an SS-PCF with an elliptical core has been proposed for analyzing different core materials' performance. Here, separately employed as core materials, gallium phosphide (GaP), graphene, and tellurite exhibit greater performance than that of earlier works. Different types of losses have been calculated here, such as confinement loss, power fraction, and numerical aperture. Numerical simulation is a crucial part that plays an important role in theoretical studies of PCF. Exploring the behaviors of the electromagnetic field within a PCF necessitated advancements in computational methods that leverage the symmetric and periodic patterns of these materials. Our investigation begins with an examination of FEM, followed by the analysis of the band structure of a PCF. The calculation of these techniques is derived from solid-state physics.

The results from the simulation of the proposed structure present modal birefringence, beat length, and power fraction for three different core materials. The research indicates that birefringence increases with wavelength. At a wavelength of  $1.5 \mu\text{m}$ , GaP shows the highest birefringence value of 0.33. High birefringence is beneficial for applications requiring strong polarization retention. Moreover, power fraction correlates with confinement loss that remains within the range of  $10^{-4} \text{ dBm}^{-1}$  to  $10^{-6} \text{ dBm}^{-1}$  for all three materials. Graphene shows the lowest confinement loss at  $0.8 \mu\text{m}$ , making it a strong candidate for long-distance communication due to its minimal signal loss. Therefore, the effective mode area also increases with wavelength which influences both NA and nonlinearity. Additionally, nonlinearity analysis shows that graphene shows the highest nonlinearity, making this fiber suitable for applications requiring high nonlinear performance, such as telecom and supercontinuum generation. The suggested SS-PCF can be utilized for a multiplicity of waveguide applications, including bandwidth propagation.

### 6.2 Future work

The numerical assessment of the suggested SS-PCF shows very promising results. In the future, my focus will be on making simple structures with small effective areas and increasing nonlinearity to enlarge the scope of applications. Additionally, I shall try to increase birefringence and minimize confinement loss to optimize signal transmission. Finally, I shall try to find a manufacturer to fabricate the proposed structure.

## 7 CONCLUSION

A new SS-PCF with a silica-rooted material formation is presented here to investigate bandwidth propagation and supercontinuum application. In this case, a FEM model with COMSOL v-5.1 of 235 430 mesh elements for the 0.1-1.5  $\mu\text{m}$  wavelength bands was used throughout the entire numerical study. The performance of different core materials, such as GaP, graphene, and tellurite, was separately studied in the SS-PCF structure. It was found that graphene has the highest nonlinearity with at least four orders of magnitude higher than the previously published values. On the other hand, all the materials provide high numerical aperture and birefringence with GaP providing the highest values. These features make the suggested SS-PCF particularly suitable for various optical fields. The strong nonlinearity of the SS-PCF could be very important for optical communication requirements, supercontinuum creation, spectroscopic systems, creating short pulses, polarization maintenance in optical fibers, and more. The SS-PCF's smooth and easily adaptable structure lends itself to efficient fabrication. Consequently, given its exceptional performance capabilities, it is probable that the suggested SS-PCF will open new avenues for future research in the realm of PCF.

## REFERENCES

- [1] J. Hecht. *City of Light: The Story of Fiber Optics*. Sloan Technology, 2004.
- [2] Stamatiou V. Kartalopoulos. *DWDM Networks, Devices, and Technology*. John Wiley & Sons Inc., USA, 2003.
- [3] J. Hecht. *Understanding Fiber Optics*. Prentice Hall, USA, 3rd edition, 1999.
- [4] Eric Udd. *Fiber Optic Sensors*. John Wiley & Sons Inc., USA, 1991.
- [5] Safa O. Kasap. *Optoelectronics and Photonics*. Pearson Education UK, 2nd edition, 2013.
- [6] Govind P. Agrawal. *Nonlinear Fiber Optics*. Academic Press, USA, 2nd edition, 1995.
- [7] Govind P. Agrawal. *Fiber-Optic Communication Systems*. John Wiley & Sons Inc., USA, 3rd edition, 2002.
- [8] R. A. Correa and J. C. Knight. Specialty fibers: Novel process eases production of hollow core fiber. *Laser Focus World*, 44(05), May 2008.
- [9] Anders Bjarklev, Jes Broeng, and Anders S. Bjarklev. *Photonic Crystal Fibers*. Kluwer Academic Press, USA, 2003.
- [10] Sajeev John. Strong localization of photons in certain disordered dielectric superlattices. *Physical Review Letters*, 58(23):2486, 1987.
- [11] Philip St. J. Russell. Photonic crystal fibers. *Science*, 299(5605):358–362, Jan. 2003.
- [12] K. Ahmed, M. Morshed, S. Asaduzzaman, and M.F.H. Arif. Optimization and enhancement of liquid analyte sensing performance based on square-cored octagonal photonic crystal fiber. *Optik-International Journal for Light and Electron Optics*, 131:687–696, 2017.
- [13] Orlando Frazao, Jose L Santos, Francisco M Araujo, and Luis A Ferreira. Optical sensing with photonic crystal fibers. *Laser & Photonics Reviews*, 2(6):449–459, 2008.
- [14] B. K. Paul, K. Ahmed, S. Asaduzzaman, and M. S. Islam. Folded cladding porous shaped photonic crystal fiber with high sensitivity in optical sensing applications: Design and analysis. *Sensing and Bio-Sensing Research*, 12:36–42, 2017.

- [15] Kawsar Ahmed, Md Shadidul Islam, and Bikash Kumar Paul. Design and numerical analysis: Effect of core and cladding area on hybrid hexagonal microstructure optical fiber in environment pollution sensing applications. *Karbala International Journal of Modern Science*, 3(1):29–38, 2017.
- [16] S. Sen, S. Chowdhury, K. Ahmed, and S. Asaduzzaman. Design of a porous cored hexagonal photonic crystal fiber based optical sensor with high relative sensitivity for lower operating wavelength. *Photonic Sensors*, 7(1):55, 2017.
- [17] M. Morshed, M. I. Hassan, T. K. Roy, M. S. Uddin, and S. A. Razzak. Microstructure core photonic crystal fiber for gas sensing applications. *Applied Optics*, 54(29):8637–8643, 2015.
- [18] M. Morshed, M. I. Hasan, and S. A. Razzak. Enhancement of the sensitivity of gas sensor based on microstructure optical fiber. *Photonic Sensors*, 5(4):312–320, 2015.
- [19] Frédéric Zolla. *Foundations of Photonic Crystal Fibres*. Imperial College Press, 2005.
- [20] Y. L. Hoo, W. Jin, J. Ju, and H. L. Ho. Numerical investigation of a depressed-index core photonic crystal fiber for gas sensing. *Sensors and Actuators B: Chemical*, 139(2):460–465, 2009.
- [21] Tanya M. Monro, D. J. Richardson, and P. J. Bennett. Developing holey fibres for evanescent field devices. *Electronics Letters*, 35(14):1188–1189, 1999.
- [22] Xia Yu, Ying Zhang, Yien Chian Kwok, and Ping Shum. Highly sensitive photonic crystal fiber based absorption spectroscopy. *Sensors and Actuators B: Chemical*, 145(1):110–113, 2010.
- [23] Jan-Michael Brosi, Christian Koos, Lucio Claudio Andreani, Michael Waldow, Juerg Leuthold, and Wolfgang Freude. High-speed low-voltage electro-optic modulator with a polymer-infiltrated silicon photonic crystal waveguide. *Optics Express*, 16(6):4177–4191, 2008.
- [24] Kiazand Fasihi. High-contrast all-optical controllable switching and routing in nonlinear photonic crystals. *Journal of Lightwave Technology*, 32(18):3126–3131, 2014.
- [25] Mohammad Arjmand and Reza Talebzadeh. Optical filter based on photonic crystal resonant cavity. *Optoelectronics and Advanced Materials-Rapid Communications*, 9(1-2):32–35, 2015.

- [26] Seung Ho Choi, Young L. Kim, and Kyung Min Byun. Graphene-on-silver substrates for sensitive surface plasmon resonance imaging biosensors. *Optics Express*, 19(2):458–466, 2011.
- [27] Jitendra Narayan Dash and Rajan Jha. Spr biosensor based on polymer pcf coated with conducting metal oxide. *IEEE Photonics Technology Letters*, 26(6):595–598, 2014.
- [28] Alireza Hassani and Maksim Skorobogatiy. Design criteria for microstructured-optical-fiber-based surface-plasmon-resonance sensors. *JOSA B*, 24(6):1423–1429, 2007.
- [29] Emmanuel K. Akowuah, Terry Gorman, Huseyin Ademgil, Shyqyri Haxha, Gary K. Robinson, and Jenny V. Oliver. Numerical analysis of a photonic crystal fiber for biosensing applications. *IEEE Journal of Quantum Electronics*, 48(11):1403–1410, 2012.
- [30] Jitendra Narayan Dash and Rajan Jha. Graphene-based birefringent photonic crystal fiber sensor using surface plasmon resonance. *IEEE Photonics Technology Letters*, 26(11):1092–1095, 2014.
- [31] Sayed Asaduzzaman, Kawsar Ahmed, Md Faizul Huq Arif, and Monir Morshed. Application of microarray-core based modified photonic crystal fiber in chemical sensing. In *Electrical & Electronic Engineering (ICEEE), IEEE, 2015 International Conference*, pages 41–44, 2015.
- [32] Sujan Chakma, Md Abdul Khalek, Bikash Kumar Paul, Kawsar Ahmed, Md Rabiul Hasan, and Ali Newaz Bahar. Gold-coated photonic crystal fiber biosensor based on surface plasmon resonance: Design and analysis. *Sensing and Bio-Sensing Research*, 18:7–12, 2018.
- [33] Philip St J Russell. Photonic-crystal fibers. *Journal of Lightwave Technology*, 24(12):4729–4749, 2006.
- [34] Xue Zhou, Shuguang Li, Tonglei Cheng, and Guowen An. Design of offset core photonic crystal fiber filter based on surface plasmon resonance. *Optical and Quantum Electronics*, 50(3):157, 2018.
- [35] X. Zhang, R. Wang, F. M. Cox, B. T. Kuhlmeiy, and M. C. J. Large. Selective coating of holes in microstructured optical fiber and its application to in-fiber absorptive polarizers. *Optics Express*, 15(24):16270–16278, 2007.

- [36] Guowen An, Shuguang Li, Wei Qin, Wan Zhang, Zhenkai Fan, and Yajie Bao. High-sensitivity refractive index sensor based on d-shaped photonic crystal fiber with rectangular lattice and nanoscale gold film. *Plasmonics*, 9(6):1355–1360, 2014.
- [37] M. Liu, H. Yuan, P. Shum, C. Shao, H. Han, and L. Chu. Simultaneous achievement of highly birefringent and nonlinear photonic crystal fibers with an elliptical tellurite core. *Applied Optics*, 57(22):6383–6387, 2018.
- [38] J. Wang. Numerical investigation of high birefringence and nonlinearity tellurite glass photonic crystal fiber with microstructured core. *Applied Optics*, 60(15):4455–4461, 2021.
- [39] S. Revathi, S. R. Inbathini, and R. A. Saifudeen. Highly nonlinear and birefringent spiral photonic crystal fiber. *Advances in OptoElectronics*, 2014.
- [40] T. Yang, E. Wang, H. Jiang, Z. Hu, and K. Xie. High birefringence photonic crystal fiber with high nonlinearity and low confinement loss. *Optics Express*, 23(7):8329–8337, 2015.
- [41] B. K. Paul, F. Ahmed, M. G. Moadar, K. Ahmed, and D. Vigneswaran. Silicon nano crystal filled photonic crystal fiber for high nonlinearity. *Optical Materials*, 84:545–549, 2018.
- [42] B. Biswas, K. Ahmed, B. K. Paul, M. A. Khalek, and M. S. Uddin. Numerical evaluation of the performance of different materials in nonlinear optical applications. *Results in Physics*, 13:102184, 2019.
- [43] K. Ahmed, B. K. Paul, M. A. Jabin, and B. Biswas. Fem analysis of birefringence, dispersion and nonlinearity of graphene coated photonic crystal fiber. *Ceramics International*, 45(12):15343–15347, 2019.
- [44] Optical Fibers Fundamentals. <https://www.meetoptics.com/academy/optical-fibers-fundamentals#optical-fiber-types>. [Accessed: 24-05-2024].
- [45] S. Revathi, S. Inabathini, and R. Sandeep. Soft glass spiral photonic crystal fiber for large nonlinearity and high birefringence. *Optica Applicata*, 45(1):15–24, 2015.
- [46] J. Liao, F. Yang, Y. Xie, X. Wang, T. Huang, Z. Xiong, and F. Kuang. Ultrahigh birefringent nonlinear slot silicon microfiber with low dispersion. *IEEE Photonics Technology Letters*, 27(17):1868–1871, 2015.

- [47] R. F. Cregan, B. J. Mangan, J. C. Knight, T. A. Birks, P. S. J. Russell, P. J. Roberts, and D. C. Allan. Single-mode photonic band gap guidance of light in air. *Science*, 285(5433):1537–1539, 1999.
- [48] T. A. Birks, J. C. Knight, and P. S. J. Russell. Endlessly single-mode photonic crystal fiber. *Optics Letters*, 22(13):961–963, 1997.
- [49] N. Granzow. Supercontinuum white light lasers: a review on technology and applications. *Photonics and Education in Measurement Science 2019*, 11144:34–38, 2019.
- [50] John M. Dudley and John R. Taylor. *Supercontinuum Generation in Optical Fibers*. Cambridge University Press, 2009.
- [51] Robert W. Boyd. *Nonlinear Optics, Third Edition*. Academic Press, 3rd edition, 2008.
- [52] Govind P. Agrawal. *Applications of Nonlinear Fiber Optics*. Academic Press, 2001.
- [53] Q. Z. Wang, D. Ji, L. Yang, P. P. Ho, and R. R. Alfano. Self-phase modulation in multimode optical fibers produced by moderately high-powered picosecond pulses. *Optics Letters*, 14(11):578–580, 1989.
- [54] Govind P. Agrawal. *Nonlinear Fiber Optics*. Academic Press, 2007.
- [55] Grant McConnell and Erling Riis. Ultra-short pulse compression using photonic crystal fibre. *Applied Physics B*, 78:557–563, 2004.
- [56] K. S. Yee. Numerical solution of initial boundary value problems involving maxwell’s equations in isotropic media. *IEEE Transactions on Antennas and Propagation*, 14(3):302–307, 1966.
- [57] A. W. Snyder and J. D. Love. *Optical waveguide theory*. Chapman and Hall, 1983.
- [58] S. G. Johnson and J. D. Joannopoulos. Block-iterative frequency-domain methods for maxwell’s equations in a planewave basis. *Optics Express*, 8(3):173–190, 2001.
- [59] O. C. Zienkiewicz, R. L. Taylor, and J. Z. Zhu. *The finite element method: its basis and fundamentals*. Elsevier, 2005.
- [60] J. M. Jin. *The finite element method in electromagnetics*. John Wiley & Sons, 2014.
- [61] T. J. R. Hughes. *The finite element method: linear static and dynamic finite element analysis*. Prentice-Hall, 1987.

- [62] R. Courant. Variational methods for the solution of problems of equilibrium and vibrations. *Lecture Notes in Pure and Applied Mathematics*, pages 1–1, 1994.
- [63] Daryl L. Logan. *A First Course in the Finite Element Method*. Cengage Learning, 2011.
- [64] P. Kumar and P. Das. Photonic crystal fiber with anomalous dispersion behavior and high birefringence. In *2015 International Conference on Applied and Theoretical Computing and Communication Technology (iCATccT)*, pages 458–461. IEEE, October 2015.
- [65] E. F. Chillcce, C. M. D. B. Cordeiro, L. C. Barbosa, and C. B. Cruz. Tellurite photonic crystal fiber made by a stack-and-draw technique. *Journal of Non-Crystalline Solids*, 352(32-35):3423–3428, 2006.
- [66] R. T. Bise and D. J. Trevor. Sol-gel derived microstructured fiber: Fabrication and characterization. In *Conference on Optical Fiber Communication, Technical Digest Series*, volume 3, pages 269–271, 2005.
- [67] M. A. Jabin, Y. Luo, G. D. Peng, M. J. Rana, K. Ahmed, T. K. Nguyen, B. K. Paul, and V. Dhasarathan. Design and fabrication of amoeba faced photonic crystal fiber for biosensing application. *Sensors and Actuators A: Physical*, 313:112204, 2020.
- [68] A. Argyros, I. M. Bassett, M. A. Van Eijkelenborg, M. C. Large, J. Zagari, N. A. Nicorovici, R. C. McPhedran, and C. M. de Sterke. Ring structures in microstructured polymer optical fibres. *Optics Express*, 9(13):813–820, 2001.
- [69] W. Wang, B. Yang, H. Song, and Y. Fan. Investigation of high birefringence and negative dispersion photonic crystal fiber with hybrid crystal lattice. *Optik-International Journal for Light and Electron Optics*, 124(17):2901–2903, 2013.
- [70] D. Vigneswaran, M.S. Mani Rajan, B. Biswas, and K. Ahmed. Exploring next generation of iot devices compatible few mode assisting ring core elliptical cladding optical fiber. *Wireless Networks*, 26(5):3217–3225, 2020.
- [71] B. Biswas, K. Ahmed, K. Ramanujam, B.K. Paul, I.S. Amiri, and W. Raja. Performance analysis of circularly photonic crystal fiber for orbital angular momentum mode generation. *Optical Engineering*, 58(8):086108–086108, 2019.
- [72] D. Vigneswaran, M.S.M. Rajan, B. Biswas, A. Grover, K. Ahmed, and B.K. Paul. Numerical investigation of spiral photonic crystal fiber (s-pcf) with supporting high order oam modes propagation for space division multiplexing applications. *Optical and Quantum Electronics*, 53:1–11, 2021.

- [73] Mortimer Abramowitz and Michael W. Davidson. Olympus microscopy resource center, Retrieved 2021-07-21.
- [74] M.M. Hassan, M.A. Kabir, M.N. Hossain, B. Biswas, B.K. Paul, and K. Ahmed. Photonic crystal fiber for robust orbital angular momentum transmission: design and investigation. *Optical and Quantum Electronics*, 52(1):8, 2020.
- [75] D. Malka, Y. Sintov, and Z. Zalevsky. Fiber-laser monolithic coherent beam combiner based on multicore photonic crystal fiber. *Optical Engineering*, 54(1):011007–011007, 2015.
- [76] D. Chen and L. Shen. Ultrahigh birefringent photonic crystal fiber with ultralow confinement loss. *IEEE Photonics Technology Letters*, 19(4):185–187, 2007.